Am J Physiol Heart Circ Physiol 292: H2809–H2816, 2007.
First published February 2, 2007; doi:10.1152/ajpheart.01176.2006.

Speckle-tracking echocardiography correctly identifies segmental left ventricular dysfunction induced by scarring in a rat model of myocardial infarction

Zoran B. Popović,[1] Carlos Benejam,[1] Jing Bian,[2] Niladri Mal,[2] Jeannie Drinko,[1] Kwangdeok Lee,[2] Farhad Forudi,[2] Rachel Reeg,[1] Neil L. Greenberg,[1] James D. Thomas,[1] and Marc S. Penn[2]

[1]*Imaging Section, Department of Cardiovascular Medicine, and* [2]*Lerner Research Institute, Departments of Cardiovascular Medicine and Stem Cell Biology, Cleveland Clinic Foundation, Cleveland, Ohio*

Submitted 26 October 2006; accepted in final form 23 January 2007

Popović ZB, Benejam C, Bian J, Mal N, Drinko J, Lee K, Forudi F, Reeg R, Greenberg NL, Thomas JD, Penn MS. Speckle-tracking echocardiography correctly identifies segmental left ventricular dysfunction induced by scarring in a rat model of myocardial infarction. *Am J Physiol Heart Circ Physiol* 292: H2809–H2816, 2007. First published February 2, 2007; doi:10.1152/ajpheart.01176.2006.—Speckle-tracking echocardiography (STE) uses a two-dimensional echocardiographic image to estimate two orthogonal strain components. The aim of this study was to assess sensitivity of circumferential (S_{circ}) and radial (S_{rad}) strains to infarct-induced left ventricular (LV) remodeling and scarring of the LV in a rat. To assess the relationship among S_{circ}, S_{rad}, and scar size, two-dimensional echocardiographic LV short-axis images (12 MHz transducer, Vivid 7 echo machine) were collected in 34 Lewis rats 4 to 10 wk after ligation of the left anterior descending artery. Percent segmental fibrosis was assessed from histological LV cross sections stained by Masson trichrome. Ten normal rats served as echocardiographic controls. S_{circ} and S_{rad} were assessed by STE. Histological data showed consistent scarring of anterior and lateral segments with variable extension to posterior and inferior segments. Both S_{circ} and S_{rad} significantly decreased after myocardial infarction ($P < 0.0001$ for both). As anticipated, S_{circ} and S_{rad} were lowest in the infarcted segments. Multiple linear regression showed that segmental S_{circ} were similarly dependent on segmental fibrosis and end-systolic diameter ($P < 0.0001$ for both), whereas segmental S_{rad} measurements were more dependent on end-systolic diameter ($P < 0.0001$) than on percent fibrosis ($P < 0.002$). STE correctly identifies segmental LV dysfunction induced by scarring that follows myocardial infarction in rats.

infarction; collagen; contractility

RECENT ADVANCES in noninvasive imaging of the left ventricle (LV) have enabled the quantification of regional function with an accuracy and simplicity that were not available previously. One of these newer methods is speckle-tracking echocardiography (STE). STE uses a standard two-dimensional echocardiographic image to estimate two orthogonal strain components (25). This method has a potential to revolutionize noninvasive assessment of regional ventricular (and possibly atrial) function (25). Although similar data can be extracted by Doppler tissue echocardiography (2), the value of this method is the freedom of the insonation angle and an ability to adopt a local coordinate system for strain measurement.

Although STE was recently validated in a variety of settings (1, 5, 10, 17, 22), the relationship of strain to underlying muscle histology is uncertain. It is unknown as to what measure a decreased strain represents muscle loss, presence of ischemia, or a simple contractility decrease. Finally, the applicability of this method to small-animal echocardiography is unknown.

The aim of this study was to assess sensitivity of circumferential (S_{circ}) and radial (S_{rad}) midwall strain components to LV remodeling and scarring induced by the myocardial infarction (MI) of the LV in a rat.

METHODS

All the animal studies reported in this article were approved by the Institutional Animal Care and Use Committee and were in compliance with the *Guide for the Care and Use of Laboratory Animals*, published by the National Institutes of Health.

Echocardiographic-histological comparisons. The data for these comparisons were gathered from animals that belonged to control groups in three treatment protocols performed at our institution. Although the study design is retrospective to original experimental protocols, the echocardiography data acquisition was performed prospectively according to standard imaging protocol in the same manner in all experiments and was identical in the studies except for the variation in the time between infarct induction and the date of euthanasia (4 vs. 10 wk). Out of these three experiments, we analyzed data sets from a total of 34 rats.

To perform these comparisons, 34 rats underwent ligation of their left anterior descending artery. Echocardiography was performed 1 to 2 days after surgery to confirm the presence of MI. After a period of 4 to 10 wk, after coronary artery ligation (or sham surgery), repeat echocardiography was performed. After this echocardiogram (2 h to 2 days), the animals were anesthetized, a hemodynamic study was performed, and animals were euthanized.

Additionally, we assessed 10 normal rats as control echocardiographic animals and 10 normal rats for control hemodynamic data acquisition.

Rat echocardiography. We used a 14-MHz linear transducer coupled to a Vivid 7 echocardiography machine (GE Medical, Milwaukee, WI) to image rats lightly sedated with ketamine (80 mg/kg ip). M-mode and two-dimensional cross-sectional echocardiography data were acquired at the papillary muscle level and digitally stored for further analysis. End-systolic diameters were calculated from the M-mode data, whereas the segmental end-diastolic wall thickness was calculated from two-dimensional data after dividing the LV into six segments using as anatomic landmarks the two insertion points of the

Address for reprint requests and other correspondence: M. S. Penn, Bakken Heart-Brain Institute, Depts. of Cardiovascular Medicine and Stem Cell Biology, Cleveland Clinic Foundation, 9500 Euclid Ave., NE3, Cleveland, OH 44195 (e-mail: pennm@ccf.org).

The costs of publication of this article were defrayed in part by the payment of page charges. The article must therefore be hereby marked "*advertisement*" in accordance with 18 U.S.C. Section 1734 solely to indicate this fact.

 0363-6135/07 $8.00 Copyright © 2007 the American Physiological Society

Downloaded from www.physiology.org/journal/ajpheart by ${individualUser.givenNames} ${individualUser.surname} (128.110.184.042) on March 24, 2018.
Copyright © 2007 American Physiological Society. All rights reserved.

right ventricular free wall and the location of posteromedial and anterolateral papillary muscles (4).

To assess midwall S_{circ} and S_{rad} and corresponding strain rates, we analyzed two-dimensional high-frame rate (frame rate range 92–123 frames/s) echocardiography data with at least 14 frames collected during each heart beat. Data were analyzed using a speckle-tracking algorithm incorporated into Echopac PC workstation (GE Medical). This recently validated (1, 5, 23) software detects and tracks the ultrasonic interference pattern (speckle) inherent to standard two-dimensional echocardiography after segmenting the ventrcular silhouette into six segments (4). Speckles are discrete hypo- and hyperechoic areas caused by the interference pattern of myocardial tissue inhomogeneities. Speckles continuously appear and disappear during the cardiac cycle due to changing tissue orientation. The size of the speckle is inversely related to the ultrasound frequency. To track speckles, a region of interest is drawn in the end-systolic frame of the cardiac cycle. Software divides the region of interest into subsegment kernels and then identifies individual speckles within every kernel by their position, size, and echogenicity. The software identifies the position of these kernels in adjacent frames by finding the region with the statistically greatest speckle similarity. Appearance and disappearance of speckles within the image are treated by Fourier autocorrelation. Local midwall tissue velocities are calculated as a shift of kernel divided by the time between frames. These two-dimensional velocity vectors are transformed from the global coordinate system of the initial image into a local one, based on the regional wall orientation, to obtain velocities in the circumferential and radial directions. Midwall strain rates are calculated by dividing the difference in velocity between two points (oriented within the local coordinate system) by their distance. Finally, strain is obtained by integrating strain rate between end diastole and end systole (defined as the occurrence of maximal and minimal LV cross-sectional area) (Fig. 1) (2, 11, 26). For each animal, end-systolic S_{circ} and S_{rad}, and corresponding peak systolic and peak early diastolic strain rates were calculated. Peak early systolic strain rate was defined as a peak strain rate occurring between end diastole and end systole. Peak early diastolic strain rate was defined as the first peak occurring after end systole. Finally, data from at least two distinct cardiac cycles were averaged.

As the variability of the echocardiographic measurements can be partitioned into software measurement error, software handling by different users, and inherent variability of the biologic signal, we estimated variability components as follows. We first measured intraobserver variability by applying speckle-tracking software twice to the same cardiac cycle in seven rats (software measurement error).

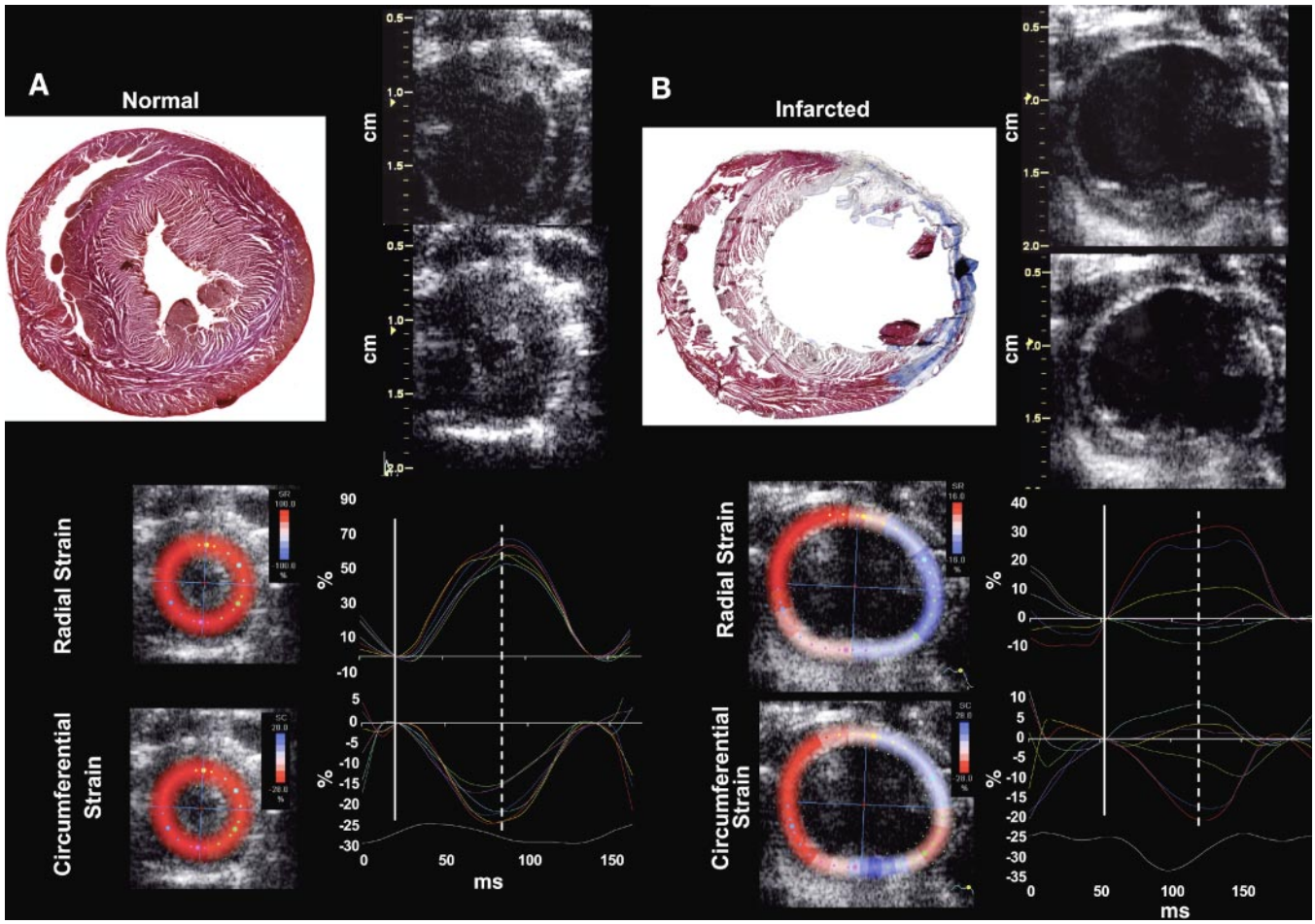

Fig. 1. *A*: an example of left ventricular cross section of the normal heart stained by Masson trichrome (*top*, *left*), echocardiographic end-diastolic and end-systolic short-axis views of the same heart (*top*, *right*), anatomic maps of end-systolic circumferential (SC) and radial (SR) strains (*bottom*, *left*), and corresponding segmental waveforms of systolic circumferential and radial strains (*bottom*, *right*; full and broken vertical lines represent end diastole and end systole, respectively). *B*: an example of left ventricular cross section of the heart with anterior myocardial infarct that shows region with replacement fibrosis in blue (*top*, *left*), corresponding echocardiographic end-diastolic and end-systolic short-axis views (*top*, *left*), corresponding anatomic maps of end-systolic circumferential and radial strains (*bottom*, *right*), and corresponding segmental waveforms of systolic circumferential and radial strains (*bottom*, *right*) that show a loss of contraction in the infarcted region. A slight mismatch between radial and circumferential strains in end systole reflects inherent method variability. Colors represent anterior (Ant, yellow), lateral (Lat, cyan), posterior (Post, green), inferior (Inf, magenta), septal (Sep, blue), and anteroseptal (A-Sep, red) walls.

Downloaded from www.physiology.org/journal/ajpheart by ${individualUser.givenNames} ${individualUser.surname} (128.110.184.042) on March 24, 2018.
Copyright © 2007 American Physiological Society. All rights reserved.

Second, we measured intraobserver variability by applying software to two consecutive cardiac cycles in 16 rats, thus measuring the combined effects of software error and biological variability. Third, two independent observers measured two different cardiac cycles, combining software error, biological signal variability, and variability in the handling of instrument. Data are presented as mean differences between measurements, as means of the absolute differences between measurements, and by the correlation coefficient.

Hemodynamic study. Rats were anesthetized by isoflurane (2–2.5%) delivered through a nasal cone. A 2-Fr microtip pressure-volume catheter (SPR-838, Millar Instruments; Houston, TX) was inserted from the right carotid artery and advanced into the LV under echocardiographic guidance (14-MHz linear transducer coupled to either Vivid 7, GE Medical or Applio, Toshiba echocardiographic machines). Data were digitally acquired at a sampling rate of 2 kHz using an RPCU-200 control unit (Millar Instruments) coupled to the National Instruments analog-to-digital converter and a personal computer. The gain and the parallel conductance of the LV volume signal were calibrated by LV end-systolic and end-diastolic volumes calculated by bullet equation from echocardiography data. In six infarcted and nine control animals, the inferior vena cava was exposed by lower right lateral thoracotomy, and the data were also collected during vena cava occlusion. All hemodynamic data were analyzed by HemoSoft software (BioCat, Cleveland, OH). After the end of the experiments, rats were euthanized with a bolus of KCl.

Histological analysis. The hearts were harvested, perfused with 10% formalin under constant pressure for 10 min, fixed in Histo-Choice (Amresco, Solon, OH), and sectioned into three equal divisions perpendicular to the LV long axis. The midventricular and apical segments were paraffin embedded according to established protocols. Tissue sections (5 μm thick) were applied to glass slides, which were dried in an oven, deparafinized in xylene, and stained with hematoxylin and eosin and Masson-trichrome stains (Fig. 1). Photomicrographs of each section were acquired using an ArtixScan 4000tf slide scanner (Microtek, Carson, CA) in conjunction with the PathScan Enabler (Meyer Instruments, Houston, TX) at a resolution of 4,000 dpi.

Infarct size was estimated from midventricular LV cross sections by quantitation of fibrillar collagen accumulation stained by Masson trichrome using ImagePro Plus (version 5.1) image analysis software. As the hearts were collected 4 to 10 wk after MI and the anterior wall had significantly thinned, the total fibrosis does not adequately reflect the infarct size induced by ligation of the left anterior descending artery. Therefore, to quantify infarct size, we measured LV circumference composed out of collagen at the epicardium and at the endocardium. After we measured total LV circumference at the epicardium and endocardium, we calculated LV infarct size as follows: Infarct size (%) = $1/2(\mathrm{Circ}_{\mathrm{coll\ endo}}/\mathrm{Circ}_{\mathrm{tot\ endo}} + \mathrm{Circ}_{\mathrm{coll\ epi}}/\mathrm{Circ}_{\mathrm{tot\ epi}})\cdot 100$, where Circ signifies circumference, coll denotes collagen, tot denotes total, and endo and epi denote endocardial and epicardial. We used the same software.

Segmental fibrosis was calculated by dividing the LV cross-sectional area at the papillary muscle level into six segments as described (4). Two independent observers graded the amount of fibrosis in percentage, and their values were then averaged. It has been previously shown that this type of fibrosis estimation corresponds well with more quantitative ways of its measurement (27). Finally, to obtain histological wall thickness, we used ImagePro Plus (version 5.1) software to first segment the LV wall as described and then to calculate average segmental wall thickness.

Statistical methods. Data are presented as means (SD). To assess registration of histology and echocardiography data, we performed within-animal correlations of end-diastolic wall thickness determined by echocardiography with both histological wall thickness and with the regional fibrosis in a total of 16 animals with transmural MI.

Statistical analyses for comparison of strains and strain rates between the animals were performed by repeated-measures analysis of variance. To assess predictors of segmental strains and strain rates, a forward stepwise multiple linear regression was used with segmental fibrosis, end-systolic diameter, and infarct age (4 vs. 10 wk) as possible predictors. The standardized β-coefficients were used as an estimate of the impact of the individual predictors on dependent variable. Finally, for comparison of hemodynamic data, we used a simple unpaired *t*-test. *P* value of <0.05 was considered significant.

RESULTS

Histological analysis demonstrated that the average size of the infarct in our animals was 31.8% (SD 14.6). Transmural myocardial infarct, defined as more than 50% fibrosis of at least one LV segment at the midventricular level, was present in 28 out of 34 rats. In 28 rats with transmural myocardial infarct, histological data showed a consistent scarring pattern with fibrosis highest in the anterior and lateral segments, decreasing toward the septum (Fig. 2*A*). There was a strong correlation between infarct size and the average segmental fibrosis ($r = 0.84$, $P < 0.001$)

Impact of transmural MI on midwall strain and strain rate. Figure 2, *B* and *C*, shows the distribution of S_{circ} and S_{rad} in control animals and animals with transmural myocardial infarct. Rats with transmural infarcts had much lower absolute values of S_{circ} and S_{rad} than controls ($P < 0.0001$ for both). In control rats, we observed a small but significant heterogeneity of S_{circ} ($P < 0.001$), whereas S_{rad} was similar in all the segments. However, in infarcted animals, there was a large heterogeneity of S_{circ} and S_{rad} ($P < 0.001$ for both), with the pattern reflecting the one seen with regional scarring. As a consequence, strain was lowest in segments with the highest fibrosis (anterior and lateral).

Figure 2, *D* and *E*, shows that peak systolic circumferential and radial strain rates were also significantly smaller in rats with transmural infarct ($P < 0.0001$ for both), with significant strain rate heterogeneity in infarcted animals ($P < 0.001$). Similarly, peak early diastolic circumferential and radial strain rates were smaller in rats with transmural infarct ($P < 0.0001$ for both), with strain rate heterogeneity in infarcted animals ($P < 0.001$) (Fig. 2, *F* and *G*).

Predictors of regional midwall segmental strain after MI. Multiple regression analysis showed that both global LV dimensions (i.e., LV end-systolic diameter) and regional fibrosis were significant predictors for S_{circ} and S_{rad}, as well as for corresponding diastolic and systolic strain rates (Table 1), with infarct age having no predictive value. Furthermore, as evidenced by the larger values of β for all strain-related parameters, global LV dimension was either similar or a stronger predictor than fibrosis, arguing against the hypothesis that any strain-related parameter is specifically coupled to regional fibrosis. Figure 3, *A* and *B*, demonstrates a strong and independent impact of end-systolic diameter and regional fibrosis on regional S_{circ} and S_{rad}.

Impact of transmural infarction on hemodynamic data and relation between strains and global LV function. In 10 controls and 24 infarcted animals (21 of which had the evidence of transmural infarct), we obtained steady-state hemodynamic data. Additionally, data during vena cava occlusion were obtained in six infarcted and nine control animals. As expected, volumes in infarcted rats were larger, contractility (evidenced by lower preload recruitable stroke work and a rightward shift of end-systolic pressure volume and stroke work/end-diastolic

Downloaded from www.physiology.org/journal/ajpheart by ${individualUser.givenNames} ${individualUser.surname} (128.110.184.042) on March 24, 2018.
Copyright © 2007 American Physiological Society. All rights reserved.

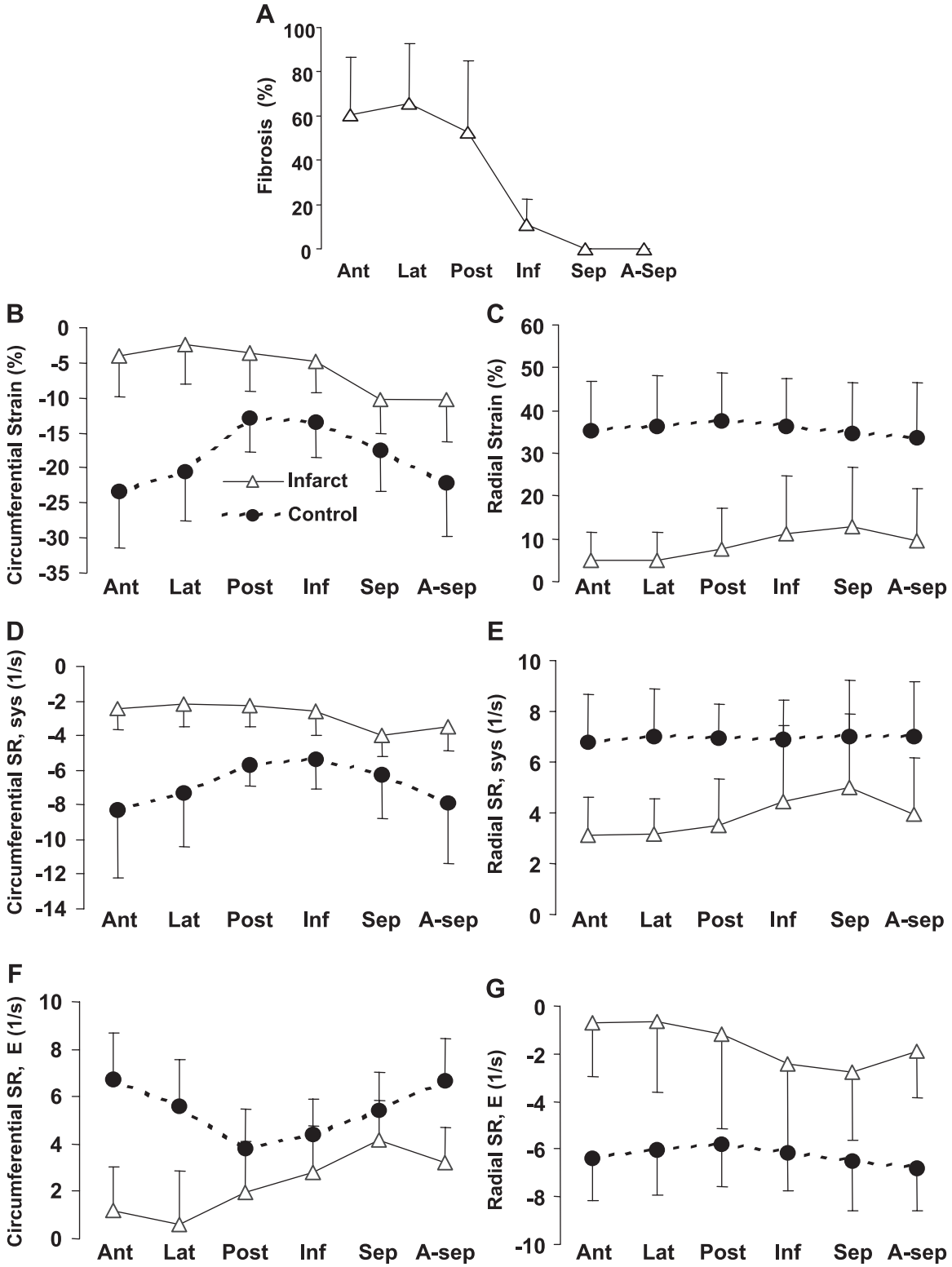

Fig. 2. *A*: distribution of segmental fibrosis in rats with transmyocardial infarction. *B* and *C*: distribution of circumferential and radial strains in rats with transmural infarct and in normal rats. *D* and *E*: distribution of circumferential and radial systolic strains rates in rats with transmural infarct and in normal rats. *F* and *G*: distribution of circumferential and radial diastolic strains rates in rats with transmural infarct and in normal rats. See text for details. SR, strain rate; Sys, systole; E, early diastole.

Downloaded from www.physiology.org/journal/ajpheart by ${individualUser.givenNames} ${individualUser.surname} (128.110.184.042) on March 24, 2018.
Copyright © 2007 American Physiological Society. All rights reserved.

Table 1. *R values and standardized β coefficients of stepwise multiple regression*

	R Value	β	
		End-systolic diameter	Percent fibrosis
S_{circ}	0.68†	0.44†	0.40†
SR_{circ}-S	0.68†	0.55†	0.26†
SR_{circ}-E	0.59†	−31†	−42†
S_{rad}	0.81†	−0.73†	−0.18†
SR_{rad}-S	0.68†	−0.57†	−0.22†
SR_{rad}-E	0.37†	0.23*	0.23*

S_{circ}, circumferential strain; S_{rad}, radial strain; SR_{circ}-S (E), S (E) wave of the circumferential strain rate; SR_{rad}-S (E), S (E) wave of the radial strain rate. *$P < 0.002$; †$P < 0.0001$.

volume relationships) was lower, and relaxation was severely impaired (Table 2).

After averaging the segmental data, we observed highly significant correlations between average S_{circ} and S_{rad} and infarct size ($r = 0.67$ and $r = -0.72$, respectively; $P < 0.001$ for both). Similarly, average early diastolic circumferential and radial strain rates correlated with infarct size ($r = -0.52$, $P = 0.003$; and $r = 0.35$, $P = 0.05$, respectively). The best hemodynamic correlate of average circumferential and radial strains was the time constant of isovolumic LV pressure decay ($r = 0.58$ and $r = -0.63$, $P < 0.002$ for both), followed by the peak negative LV pressure derivative ($r = 0.49$ and $r = -0.52$, $P < 0.02$ for both), with LV end-diastolic pressure showing a borderline inverse relationship with S_{rad} only ($r = -0.41$, $P = 0.04$). Surprisingly, peak positive LV pressure derivative did not show significant correlation with either of the average strains. Similar results were obtained for the average of early diastolic radial and circumferential strain rates.

Intraobserver variability and registration of echocardiography and histology data. Intra- and interobserver variability data are presented in Table 3. The average within-animal correlation coefficient for the relation between echocardiographic end-diastolic wall thickness and histological wall thickness was $r = 0.59$ (SD 0.17) (supplemental Fig. 1*A*; note: supplemental figure may be found through a link in the online version of this article). End-diastolic wall thickness underestimated histological wall thickness by 0.29 mm (SD 0.66) ($P = 0.003$). The average within-animal correlation coefficient for the relation between end-diastolic wall thickness and regional fibrosis was $r = -0.75$ (SD 0.14) (supplemental Fig. 1*B*).

DISCUSSION

In this article we show that LV midwall end-systolic strains measured by STE reflect two basic processes that occur after MI: replacement fibrosis and adverse LV remodeling. As a result, no simple cutoff point for the values of end-systolic strains can be assumed to differentiate between healthy and diseased myocardium; rather, a global function must be incorporated into the equation.

Several articles have assessed the sensitivity of strain (or strain rate) measured either by magnetic resonance or Doppler tissue imaging to detect viable myocardium after MI (3, 28, 30). However, to our knowledge, this is the first study that shows the way that regional fibrosis interacts with LV remodeling to influence segment function. This study extends the findings of Park et al. (19) who showed that fibrosis and end-systolic stress adversely affect diastolic strain rates, although they did not quantify their relative contributions. In the current article we show this interaction in a relatively large series of small animals using a novel noninvasive technology.

Impact of infarct on strain distribution in the rat ventricle. The two fundamental processes that occur after large anterior MI and that are responsible for the occurrence of heart failure, arrhythmias, and death are replacement fibrosis and LV dilation through adverse remodeling. In theory, replacement fibrosis affects strain through loss of contractile elements, whereas remodeling affects strain through increased stress (afterload) (15) and decreased contractility of remaining myocytes (9). In concordance with our study, a recent article has demonstrated that peak-systolic and early diastolic strain rates, which closely correlate with strain, show strong dependence on the development of postmyocardial fibrosis (19).

In contrast, the relationship between end-systolic dimensions and strain post-MI is not well documented. However, this relationship is quite obvious because of the interplay among regional stress, strain, and systolic myocardial stiffness. Regional stress represents the total force in a given direction per unit area normal to that direction (21), whereas systolic myocardial stiffness (i.e., contractility) can be described mathematically as the change in stress divided by the change in strain (13, 16). Thus, with a constant contractility assumed, an increase in stress must lead to a decrease in strain. Stress, in turn, is determined by local radii of curvature (21, 29), which for radial and meridional stress can be approximated by end-systolic diameters (8). As a confirmation, Bogaert et al. (3) used magnetic resonance imaging to show that strains decrease in the remote regions after myocardial infarct and that this decrease is associated with increased circumferential and longitudinal radii of curvature (3). Interestingly, a recent clinical article found no correlation between end-systolic volume and longitudinal strain measured by Doppler tissue imaging post-MI. This possibly reflects limitations of tissue Doppler strain rate measurement or relatively preserved end-systolic volumes after reperfused MI (30). In our article, we clearly show the interdependence of strain and end-systolic diameter. Since systolic cross-sectional LV shape corresponds roughly to a circle, end-systolic diameter is a good approximation of the radius of circumferential curvature, which in turn is a major determinant of systolic stress.

The practical consequence of this finding is that one cannot use a single cutoff value for strain to determine the amount of fibrosis or viability or just as a simple surrogate for the visual assessment of wall motion; rather, any regional strain measure has to be corrected for global end-systolic LV dimensions.

Measuring strain components by STE. Unlike ejection fraction that expresses a deformation (decrease) of ventricular volume as a single number, strain is an antisymmetric 3×3 tensor, meaning that it is composed of six interdependent components that reflect tissue deformation occurring along specific axes of a specified coordinate system. STE is a recently developed tool that tracks interference patterns from subwavelength structures to characterize segmental muscle movement (25). STE simultaneously measures strain in two (and potentially three) (12) orthogonal directions from a single echocardiographic view, while using local coordinate systems

Downloaded from www.physiology.org/journal/ajpheart by ${individualUser.givenNames} ${individualUser.surname} (128.110.184.042) on March 24, 2018.
Copyright © 2007 American Physiological Society. All rights reserved.

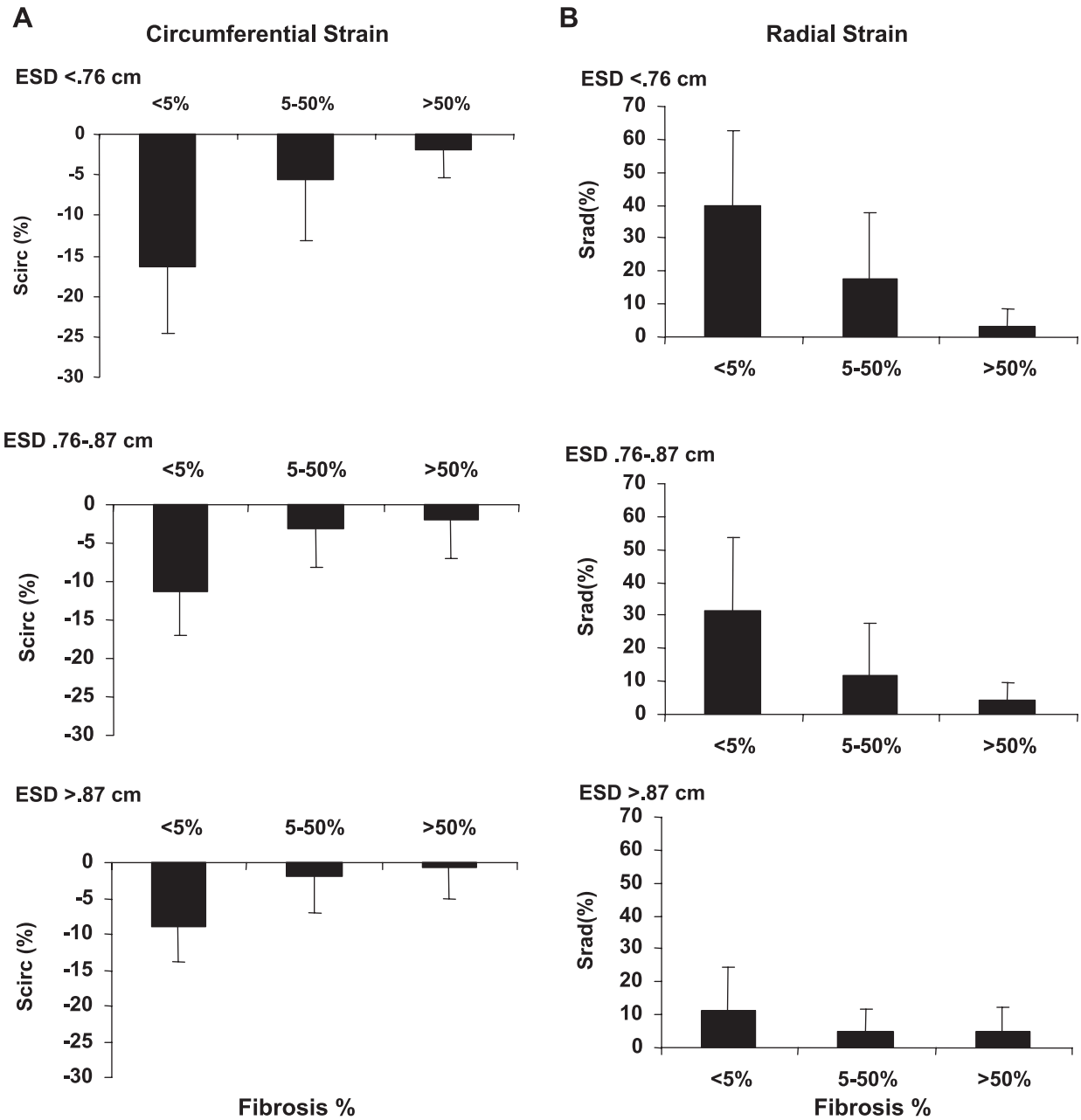

Fig. 3. Regional strains in circumferential (S_{circ}; *A*) and radial orientation (S_{rad}; *B*) according to tertiles of end-systolic diameter (ESD) and the degree of regional fibrosis. Absolute strain values decrease with increasing levels of fibrosis and of end-systolic diameter. See text for details.

defined by neighboring ventricular shape. This makes it superior to the strain assessment by Doppler tissue echocardiography, with its known angle dependence and the ability to assess only one component of strain at a time. Several articles validated various strain components by STE against sonomicrometry and magnetic resonance imaging (1, 5, 22). Of note, although in clinical echocardiography frame rates of >90 frames/s often lead to poor speckle tracking (23), they are necessary in rodents due to their high heart rate. Speckle-tracking quality depends on scan line resolution, which in turn depends on transducer frequency, sector width and depth, and the number of crystals within the transducer. Since our 14-MHz linear transducer generates images using high crystal density over a very small sector width and depth, it was possible to obtain good tracking at high frame rates without the loss of scan line resolution.

However, STE expresses LV function in a specific region, not as a single value but as a set of multiple, possibly divergent, measures. Thus the question emerges, Is it necessary to measure more than one component of strain since it is known that these components are cross-correlated? In addition, if the strain values are divergent, which one is the most sensitive to particular physiological process? Our multiple regression analysis data indicate that, in a same segment, circumferential strain is more sensitive to presence of fibrosis, whereas radial strain depends more on LV geometry (a surrogate of end-systolic stress).

Regional strain heterogeneity. We have shown that even normal animals show strain heterogeneity as assessed by STE,

Downloaded from www.physiology.org/journal/ajpheart by ${individualUser.givenNames} ${individualUser.surname} (128.110.184.042) on March 24, 2018.
Copyright © 2007 American Physiological Society. All rights reserved.

Table 2. *Hemodynamic data in rats with transmural MI and controls*

	Transmural MI	Controls
R-R interval, ms	213.31 (SD 28.67)	187.68 (SD 19.33)*
LV EDV, ml	1.08 (SD 0.41)	0.37 (SD 0.11)†
LV ESV, ml	0.84 (SD 0.35)	0.18 (SD 0.06)†
LV P_{max}	88.06 (SD 16.17)	89.5 (SD 14.93)
LV EDP, mmHg	14.25 (SD 8.51)	7.84 (SD 4.03)*
dP/dt_{max}, mmHg/s	3,836 (SD 1,293)	4,258 (SD 1,540)
dP/dt_{min}, mmHg/s	−3,162 (SD 1,050)	−4,507 (SD 1,727)†
Stroke work, mmHg·ml	25.66 (SD 19.67)	18.69 (SD 9.52)
τ, ms	17.36 (SD 3.52)	10.89 (SD 1.89)†
E_{es}, mmHg/ml	297.51 (SD 101.35)	508.56 (SD 368.03)
PRSW, mmHg	64.57 (SD 8.57)	84.76 (SD 12.86)*
V_0, ml	0.23 (SD 0.27)	−0.04 (SD 0.11)*
V_w, ml	0.39 (SD 0.21)	0.15 (SD 0.05)†

Values are means (SD). MI, myocardial infarction; LV, left ventricular; EDV, end-diastolic volume; ESV, end-systolic volume; P_{max}, maximal systolic pressure; EDP, end-diastolic pressure; dP/dt_{max}, first derivative of maximum pressure; dP/dt_{min}, first derivative of minimum pressure; τ, time constant of isovolumic pressure decay; E_{es}, end-systolic elastance; PRSW, preload recruitable stroke work; V_0, *x*-axis intercept of end-systolic pressure-EDV relationships; V_w, *x*-axis intercept of stroke work-EDV relationships. *$P < 0.05$; †$P < 0.01$.

with the inferior wall showing the lowest circumferential strain. In contrast, only a nonsignificant trend was noted with radial strain being slightly higher in inferior region. This is possibly due to technical reasons, and further studies are needed to elucidate this. However, Sun et al. (24) and Moore et al. (14) showed that normal volunteers have lower strains in the inferior and septal, as opposed to the anterior and lateral, walls. Since LV structure between mammalian species is essentially identical (6, 7), some strain heterogeneity should also be expected in rodents. This indicates that different "normal" values have to be used for different segments.

Are diastolic or systolic function parameters more sensitive to ventricular structure? Both contractility and relaxation are tightly coupled to ventricular structure and to each other through calcium handling. For example, dobutamine simultaneously increases contractility and decreases the time constant of relaxation. Still, there may be a difference in the sensitivity of contractility versus relaxation parameters. In this article, we show that the presence of chronic MI (and thus of replacement fibrosis) affected the peak-negative LV pressure derivative more than it did peak-positive LV pressure derivative. However, we have not corroborated the findings of Park et al. (19) that early diastolic strain rates (whether radial or circumferential) are more sensitive to fibrosis or LV remodeling than systolic strain rates or strains. A possible reason may be because of a fusion of E and A waves of the strain-rate signal in rats or to a slow frame rate.

Clinical implications. Several articles have stressed the correlation between regional wall motion and strain (5, 11) to facilitate wall motion scoring. This article indicates that specific cutoff values of strain cannot be used as surrogates of "viability" since low strain can occur in the presence of LV remodeling, even in the regions remote from the myocardial infarct. Another finding is that the areas of very prominent negative strain (i.e., dyskinesis) were not frequently observed. This probably reflects the fact that replacement fibrosis has a very high tensile strength, resisting any passive change in systole.

Limitations. Several limitations should be kept in mind when assessing the results of this study. Strain is a three-dimensional tensor, whereas our method quantifies myocardial deformation in a two-dimensional plane. Also, the frame rate relative to heart cycle duration used in this study was lower than in previous ones performed in humans or large animals (1). However, it should be pointed out that in small animals, since the relative duration of LV filling is shorter, systole lasts as long as or even longer than diastole (20). Thus we had seven to eight systolic frames to reconstruct a systolic part of the strain curve, a number that was very similar to the eight frames that were available to us for a similar task in a recent human magnetic resonance tagging study (18). Additionally, because we did not infuse the paraffin into the hearts under end-diastolic pressure and because some distortional effects of dehydration and shrinkage associated with embedding could not be avoided, our histological measures of wall thickness do not exactly reflect in vivo end-diastolic thickness. Still, satisfactory within-animal correlation between histological and in vivo measured wall thickness was obtained.

Depressed strain in remote regions of the infracted animals may be due to ketamine effects. However, ketamine dosage was kept to a minimum with the aim of inducing sedation only. Also, both normal controls and MI groups were treated in the identical manner, and thus differences between groups in

Table 3. *Intra- and interobserever variability for circumferential and radial strain and strain rate data*

	Circumferential			Radial		
Variability	Strain, %	SR S, 1/s	SR E, 1/s	Strain, %	SR S, 1/s	SR E, 1/s
Intraobserver, same cycle						
Mean Abs Diff	2.7 (SD 2.2)	0.79 (SD 0.74)	1.2 (SD 1.13)	8.6 (SD 6.8)	1.66 (SD 1.35)	1.5 (SD 1.17)
Mean Diff	−0.2 (SD 3.5)	0.07 (SD 1.09)	0.36 (SD 1.62)	−5.2 (SD 9.70)	1.47 (SD 1.56)	−1.19 (SD 1.5)
Correlation	0.89	0.90	0.80	0.93	0.89	0.82
Intraobserver, different cycles						
Mean Abs Diff	3.6 (SD 2.6)	1.33 (SD 1.24)	1.49 (SD 1.31)	9.0 (SD 6.0)	2.22 (SD 2.18)	1.71 (SD 1.78)
Mean Diff	0.3 (SD 4.5)	−0.1 (SD 1.82)	0.09 (SD 1.99)	−0.7 (SD 10.8)	−1.25 (SD 2.86)	0.14 (SD 2.47)
Correlation	0.86	0.80	0.72	0.88	0.74	0.72
Interobserver, different cycles						
Mean Abs Diff	4.8 (SD 3.6)	1.59 (SD 1.64)	2.06 (SD 2.53)	10.6 (SD 6.1)	2.08 (SD 1.78)	1.95 (SD 1.47)
Mean Diff	1.8 (SD 5.8)	−0.11 (SD 2.3)	−0.2 (SD 3.27)	−3.8 (SD 11.7)	−0.59 (SD 2.7)	−0.67 (SD 2.37)
Correlation	0.75	0.65	0.40	0.88	0.69	0.57

Values are means (SD). Abs, absolute; Diff, difference; E, early diastolic; S, systolic; SR, strain rate.

Downloaded from www.physiology.org/journal/ajpheart by ${individualUser.givenNames} ${individualUser.surname} (128.110.184.042) on March 24, 2018.
Copyright © 2007 American Physiological Society. All rights reserved.

noninfarcted segments were obtained under the same physiological conditions. Finally, rats are able to withstand huge myocardial infarcts, and thus, very frequently, the infracted territories in our experiments were large. It is questionable how this relates to human infarcts, especially in the early reperfusion era.

In conclusion, STE can correctly identify segmental LV dysfunction induced by scarring in a rat model of MI. Regional midwall strain is influenced by both global remodeling and regional fibrosis.

GRANTS

This study was supported by National Heart, Lung, and Blood Institute Grant R01-HL-74400-01; the National Space Biomedical Research Institute through NASA Grant NCC-9-58 (Houston, TX); and the Department of Defense Grant 02360007 (Ft. Dietrick, MD).

REFERENCES

1. **Amundsen BH, Helle-Valle T, Edvardsen T, Torp H, Crosby J, Lyseggen E, Stoylen A, Ihlen H, Lima JA, Smiseth OA, Slordahl SA.** Noninvasive myocardial strain measurement by speckle tracking echocardiography validation against sonomicrometry and tagged magnetic resonance imaging. *J Am Coll Cardiol* 47: 789–793, 2006.
2. **Askari AT, Unzek S, Popovic ZB, Goldman CK, Forudi F, Kiedrowski M, Rovner A, Ellis SG, Thomas JD, DiCorleto PE, Topol EJ, Penn MS.** Effect of stromal-cell-derived factor 1 on stem-cell homing and tissue regeneration in ischaemic cardiomyopathy. *Lancet* 362: 697–703, 2003.
3. **Bogaert J, Bosmans H, Maes A, Suetens P, Marchal G, Rademakers FE.** Remote myocardial dysfunction after acute anterior myocardial infarction: impact of left ventricular shape on regional function: a magnetic resonance myocardial tagging study. *J Am Coll Cardiol* 35: 1525–1534, 2000.
4. **Cerqueira MD, Weissman NJ, Dilsizian V, Jacobs AK, Kaul S, Laskey WK, Pennell DJ, Rumberger JA, Ryan T, Verani MS.** Standardized myocardial segmentation and nomenclature for tomographic imaging of the heart: a statement for healthcare professionals from the Cardiac Imaging Committee of the Council on Clinical Cardiology of the American Heart Association. *Circulation* 105: 539–542, 2002.
5. **Cho GY, Chan J, Leano R, Strudwick M, Marwick TH.** Comparison of two-dimensional speckle and tissue velocity based strain and validation with harmonic phase magnetic resonance imaging. *Am J Cardiol* 97: 1661–1666, 2006.
6. **Costa KD, May-Newman K, Farr D, O'Dell WG, McCulloch AD, Omens JH.** Three-dimensional residual strain in midanterior canine left ventricle. *Am J Physiol Heart Circ Physiol* 273: H1968–H1976, 1997.
7. **Grimm AF, Katele KV, Lin HL.** Fiber bundle direction in the mammalian heart. An extension of the "nested shells" model. *Basic Res Cardiol* 71: 381–388, 1976.
8. **Grossman W, Jones D, McLaurin LP.** Wall stress and patterns of hypertrophy in the human left ventricle. *J Clin Invest* 56: 56–64, 1975.
9. **Guccione JM, Moonly SM, Moustakidis P, Costa KD, Moulton MJ, Ratcliffe MB, Pasque MK.** Mechanism underlying mechanical dysfunction in the border zone of left ventricular aneurysm: a finite element model study. *Ann Thorac Surg* 71: 654–662, 2001.
10. **Helle-Valle T, Crosby J, Edvardsen T, Lyseggen E, Amundsen BH, Smith HJ, Rosen BD, Lima JA, Torp H, Ihlen H, Smiseth OA.** New noninvasive method for assessment of left ventricular rotation: speckle tracking echocardiography. *Circulation* 112: 3149–3156, 2005.
11. **Leitman M, Lysyansky P, Sidenko S, Shir V, Peleg E, Binenbaum M, Kaluski E, Krakover R, Vered Z.** Two-dimensional strain-a novel software for real-time quantitative echocardiographic assessment of myocardial function. *J Am Soc Echocardiogr* 17: 1021–1029, 2004.
12. **Meunier J.** Tissue motion assessment from 3D echographic speckle tracking. *Phys Med Biol* 43: 1241–1254, 1998.
13. **Mirsky I, Tajimi T, Peterson KL.** The development of the entire end-systolic pressure-volume and ejection fraction-afterload relations: a new concept of systolic myocardial stiffness. *Circulation* 76: 343–356, 1987.
14. **Moore CC, Lugo-Olivieri CH, McVeigh ER, Zerhouni EA.** Three-dimensional systolic strain patterns in the normal human left ventricle: characterization with tagged MR imaging. *Radiology* 214: 453–466, 2000.
15. **Moustakidis P, Maniar HS, Cupps BP, Absi T, Zheng J, Guccione JM, Sundt TM, Pasque MK.** Altered left ventricular geometry changes the border zone temporal distribution of stress in an experimental model of left ventricular aneurysm: a finite element model study. *Circulation* 106: I168–I175, 2002.
16. **Nakano K, Sugawara M, Ishihara K, Kanazawa S, Corin WJ, Denslow S, Biederman RW, Carabello BA.** Myocardial stiffness derived from end-systolic wall stress and logarithm of reciprocal of wall thickness. Contractility index independent of ventricular size. *Circulation* 82: 1352–1361, 1990.
17. **Notomi Y, Lysyansky P, Setser RM, Shiota T, Popovic ZB, Martin-Miklovic MG, Weaver JA, Oryszak SJ, Greenberg NL, White RD, Thomas JD.** Measurement of ventricular torsion by two-dimensional ultrasound speckle tracking imaging. *J Am Coll Cardiol* 45: 2034–2041, 2005.
18. **Notomi Y, Setser RM, Shiota T, Martin-Miklovic MG, Weaver JA, Popovic ZB, Yamada H, Greenberg NL, White RD, Thomas JD.** Assessment of left ventricular torsional deformation by Doppler tissue imaging: validation study with tagged magnetic resonance imaging. *Circulation* 111: 1141–1147, 2005.
19. **Park TH, Nagueh SF, Khoury DS, Kopelen HA, Akrivakis S, Nasser K, Ren G, Frangogiannis NG.** Impact of myocardial structure and function postinfarction on diastolic strain measurements: implications for assessment of myocardial viability. *Am J Physiol Heart Circ Physiol* 290: H724–H731, 2006.
20. **Popovic ZB, Richards KE, Greenberg NL, Rovner A, Drinko J, Cheng Y, Penn MS, Fukamachi K, Mal N, Levine BD, Garcia MJ, Thomas JD.** Scaling of diastolic intraventricular pressure gradients is related to filling time duration. *Am J Physiol Heart Circ Physiol* 291: H762–H769, 2006.
21. **Regen DM, Nonogi H, Hess OM.** Estimation of left-ventricular systolic performance and its determinants in man from pressures and dimensions of one beat: effects of aortic valve stenosis and replacement. *Heart Vessels* 6: 31–47, 1990.
23. **Suffoletto MS, Dohi K, Cannesson M, Saba S, Gorcsan J 3rd.** Novel speckle-tracking radial strain from routine black-and-white echocardiographic images to quantify dyssynchrony and predict response to cardiac resynchronization therapy. *Circulation* 113: 960–968, 2006.
24. **Sun JP, Popovic ZB, Greenberg NL, Xu XF, Asher CR, Stewart WJ, Thomas JD.** Noninvasive quantification of regional myocardial function using Doppler-derived velocity, displacement, strain rate, and strain in healthy volunteers: effects of aging. *J Am Soc Echocardiogr* 17: 132–138, 2004.
25. **Thomas JD, Popovic ZB.** Assessment of left ventricular function by cardiac ultrasound. *J Am Coll Cardiol* 48: 2012–2025, 2006.
26. **Thomas JD, Popovic ZB.**Speckle tracking echocardiography. In: *Braunwald's Heart Disease* (7th ed.), edited by Zipes DP, Libby P, Bonow RO, and Braunwald E. Amsterdam: Elsevier, 2006.
27. **Vasiljevic JD, Popovic ZB, Otasevic P, Popovic ZV, Vidakovic R, Miric M, Neskovic AN.** Myocardial fibrosis assessment by semiquantitative, point-counting and computer-based methods in patients with heart muscle disease: a comparative study. *Histopathology* 38: 338–343, 2001.
28. **Weidemann F, Dommke C, Bijnens B, Claus P, D'Hooge J, Mertens P, Verbeken E, Maes A, Van de Werf F, De Scheerder I, Sutherland GR.** Defining the transmurality of a chronic myocardial infarction by ultrasonic strain-rate imaging: implications for identifying intramural viability: an experimental study. *Circulation* 107: 883–888, 2003.
29. **Wong AY, Rautaharju PM.** Stress distribution within the left ventricular wall approximated as a thick ellipsoidal shell. *Am Heart J* 75: 649–662, 1968.
30. **Zhang Y, Chan AK, Yu CM, Yip GW, Fung JW, Lam WW, So NM, Wang M, Wu EB, Wong JT, Sanderson JE.** Strain rate imaging differentiates transmural from non-transmural myocardial infarction: a validation study using delayed-enhancement magnetic resonance imaging. *J Am Coll Cardiol* 46: 864–871, 2005.

Downloaded from www.physiology.org/journal/ajpheart by ${individualUser.givenNames} ${individualUser.surname} (128.110.184.042) on March 24, 2018.
Copyright © 2007 American Physiological Society. All rights reserved.